Marine and Petroleum Geology 129 (2021) 105069

Contents lists available at ScienceDirect

Marine and Petroleum Geology

journal homepage: www.elsevier.com/locate/marpetgeo

Fractal behaviors of NMR saturated and centrifugal T_2 spectra in oil shale reservoirs: The Paleogene Funing formation in Subei basin, China

Xiaoping Liu [a,b,*], Zhijun Jin [c,d], Jin Lai [a,b], Xuechun Fan [b], Ming Guan [b], Honglin Shu [e], Gaocheng Wang [e], Mengcai Liu [e], Yufeng Luo [e]

[a] State Key Laboratory of Petroleum Resources and Prospecting, China University of Petroleum (Beijing), Beijing, 102249, China
[b] College of Geosciences, China University of Petroleum (Beijing), Beijing, 102249, China
[c] Institute of Energy, Peking University, Beijing, 100871, China
[d] State Key Laboratory of Shale Oil and Gas Enrichment Mechanisms and Effective Development, Beijing, 100083, China
[e] Research Institute of Petroleum Exploration Development, PetroChina Zhejiang Oilfield Company, Hangzhou, Zhejiang, China

ARTICLE INFO

Keywords:
Fractal
Oil shale
Pore structure
T_2 spectrum
NMR measurements
Funing formation
Subei basin

ABSTRACT

Fluorescence thin section and scanning electron microscopy (SEM) analysis were performed to delineate pore spaces and pore network assemblages of oil shales of Member 2 of Paleogene Funing Formation (E_1f_2) in Subei Basin, China. Nuclear magnetic resonance (NMR) T_2 (transverse relaxation time) spectra were used to gain insight into pore size distribution. Fractal analysis was performed on the NMR T_2 spectra measured at saturated and centrifugal status, respectively, with the aim to reveal the different fractal behaviors of irreducible pore realms (centrifugal T_2 spectrum) and the entire pore systems (saturated T_2 spectrum). Relationships between NMR parameters and fractal dimensions were revealed. The results show that the pore spaces consist of 1) large pore realms including interparticle pores, and microfractures, 2) small pore realms including intragranular dissolution pores, intercrystal micropores and organic matter pores. The T_2 spectra are mostly bimodal and left-skewed due to abundance in small pore realms. The right peak or tail distribution is associated with large pore realms. Fractal analysis performed on saturated and centrifugal T_2 spectra show that fractal dimensions calculated from centrifugal T_2 spectrum are higher. In addition, fractal dimensions for centrifugal T_2 spectrum show negative correlation relationships with BVI and $T_{2cutoff}$ values. The different fractal behaviors of saturated and centrifugal T_2 spectra reflect the complex pore assemblages in oil shales. The small pore realms determine the microscopic complexity, while large pore realms control the macroscopic reservoir quality of oil shales. However large pore realms (interparticle pores and micro-fractures) are not self-similar with the small pore realms, and can't be described by fractal dimension. Fractal analysis gives insights in the heterogeneous assemblage of pore systems and helps describe complexity of pore structure.

1. Introduction

Shale oil reservoirs, which contain pore systems ranging from the nanoscale up to the macroscale, have ultra-low porosity (<10%) and in situ permeability (<0.1 mD) (Loucks et al., 2009; Curtis et al., 2012; Yan et al., 2018; Yang et al., 2019; Li et al., 2019; Liu et al., 2020). The Paleogene Funing Formation (member 2) in Subei Basin is a typical organic matter-rich oil shale (Zhang et al., 2014), of which the lithology are dark gray–black shales interbedded with carbonate and marls, and recently abundant shale oils have been produced (Cheng et al., 2019; Liu et al., 2020). The Paleogene Funing Formation oil shales have various pore spaces and complex pore throat assemblages (Liu et al., 2020). Therefore quantitative evaluation of pore structure is critical for the resource potential evaluation and effective exploitation of shale oil (Zhang et al., 2017; Liu et al., 2020).

Pore space assemblage and microscopic pore throat structures determine macroscopic petrophysical parameters, petroleum charging, migration, and accumulation in oil shales (Schmitt et al., 2015; Tan et al., 2017; Li et al., 2016; Zhao et al., 2017a,b,c; Zhang et al., 2017; Wang et al., 2019; Guan et al., 2020). However, pore structure in oil shales is difficult to be quantitatively described due to various pore spaces and complex pore assemblage, and various complementary

* Corresponding author. China University of Petroleum (Beijing), 18 Fuxue Road, Changping, Beijing, 102249, China.
E-mail address: liuxiaoping@cup.edu.cn (X. Liu).

https://doi.org/10.1016/j.marpetgeo.2021.105069
Received 6 October 2020; Received in revised form 10 March 2021; Accepted 3 April 2021
Available online 9 April 2021

techniques need to be used to fully characterize the entire pore size spectra (Li et al., 2017; Zhang et al., 2018; Liu et al., 2020; Guan et al., 2020). In addition, fractal theory should be incorporated to comprehensively characterize the geometric shapes, pore throat size and distributions in oil shales (Zhao et al., 2017a,b,c; Zhang et al., 2018; Yan et al., 2020; Guan et al., 2020). Fractals are geometrical objects which are self-similar and appear independent of scales (Anovitz et al., 2013; Kulesza and Bramowicz, 2014; Wang et al., 2018). Fractal geometry has been widely used to evaluate the heterogeneity of reservoir rocks since its initially being proposed, and fractal theory helps build up relationships between micro-morphology and macroscopic performance (Kleinberg et al., 1994; Li and Horne, 2006; Cai et al., 2010, 2017; Xie et al., 2010; Li, 2010; Hu et al., 2012; Wang et al., 2012; Lai et al., 2016; Daigle and Johnson, 2016). Through fractal analysis of NMR T_2 spectra, insights can be provided in the heterogeneous pore assemblage and complexity of pore structure in oil shale reservoirs.

The main goals of this study are to investigate the pore spaces, NMR pore size distribution, pore assemblage, and fractal behaviors of the Funing Formation oil shales in Subei Basin using a combination of thin sections, SEM analysis and NMR T_2 spectrum (Fig. 1). The pore spaces and their oil bearing property were firstly investigated by fluorescence thin sections and SEM analysis. Then the pore size distributions are determined from NMR T_2 spectra measured at saturated and centrifugal status, respectively. Internal relationships between reservoir quality and NMR parameters such as $T_{2cutoff}$ and BVI values are investigated. Fractal analysis was then performed on the NMR T_2 spectra at the measured at saturated and centrifugal status, and the fractal dimensions are derived from the fractal curves, respectively. At last the fractal behaviors and implications for pore structure evaluation were discussed. The work is hoped to provide insights into heterogeneous assemblage of pore systems, and also helps extend the application of NMR measurements in fractal analysis for oil shale reservoirs worldwide (see Fig. 1).

2. Theories and analytical methods

2.1. Theory

In NMR measurements, a T_2 (transverse relaxation time) spectrum or T_2 relaxation time distribution, of which the x-axis is T_2 value, and the y-axis are (incremental and cumulative) pore volumes corresponding to each T_2 value (Fig. 2; Fig. 3A).

The pore size distribution (T_2 distribution) in porous rocks can be described by a fractal model (Li and Horne, 2003; Wang et al., 2012, 2018; Jin et al., 2013; Daigle et al., 2014b; Gao et al., 2014; Lai et al., 2018). In this model, the cumulative pore volume Vp and T_2 can be expressed as Eq. (1) (Daigle et al., 2014a; Zhao et al., 2017a,b,c; Zhang et al., 2020). Eq. (1) can be further written as Eq. (2) (Zhang et al., 2003; Zhang and Weller, 2014, Zhou and Kang, 2016, and Zhao et al., 2017a,b, c).

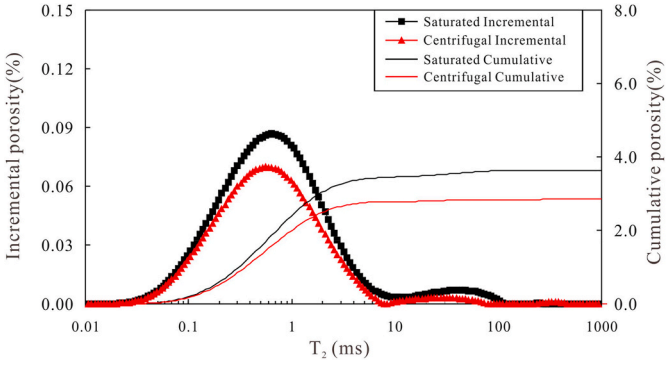

Fig. 2. Typical NMR T_2 spectrum of oil shale of Funing Formation in Subei Basin.

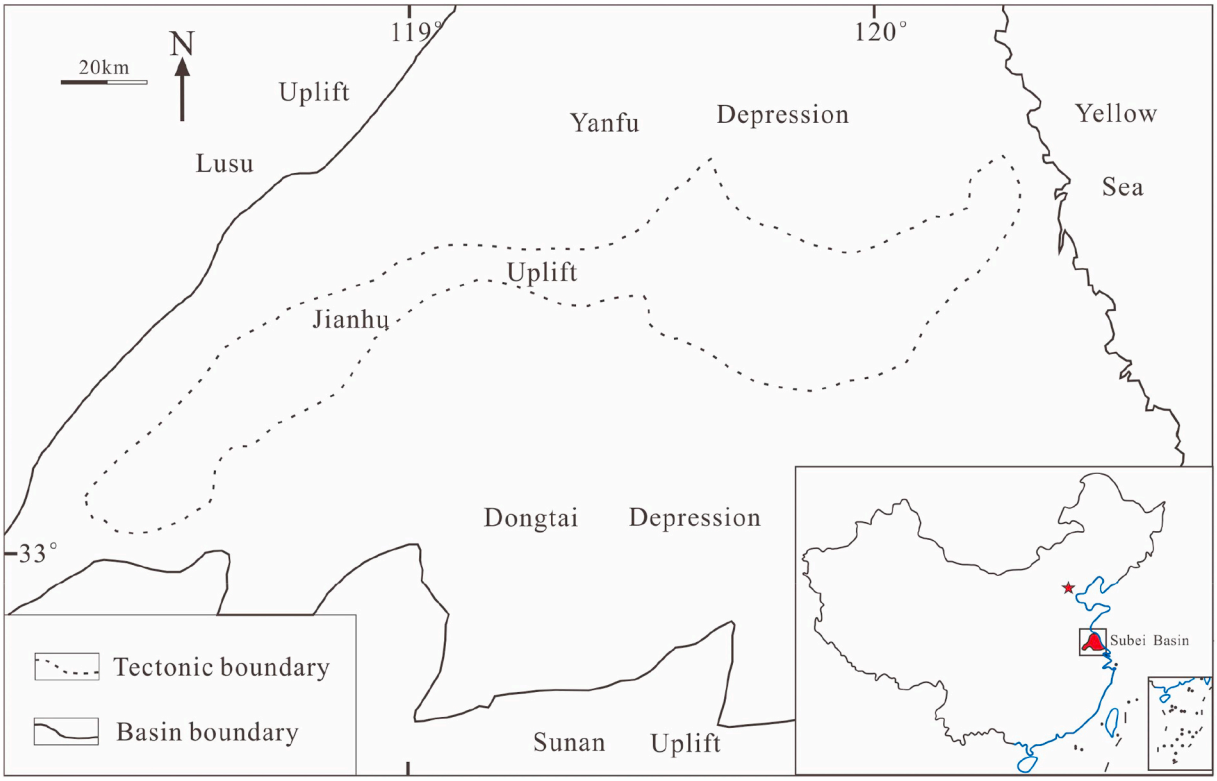

Fig. 1. The tectonic division of Subei Basin (Zhang et al., 2014; Liu et al., 2012; Liu et al., 2020).

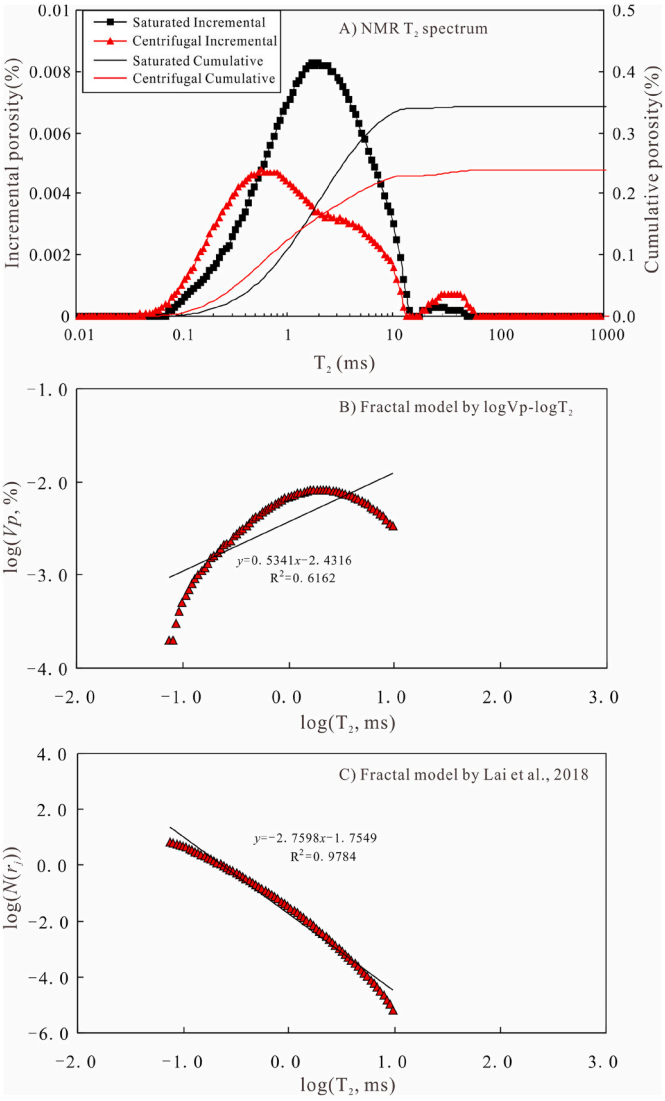

Fig. 3. Two different fractal model to derive fractal dimension from NMR T_2 spectra in oil shales of Funing Formation in Subei Basin. A. NMR T_2 spectrum. B. The curve log(Vp) versus log(T_2). C. Using fractal model proposed by Lai et al., (2018) to derive fractal dimension.

$$V_p = \left(\frac{T_2}{T_{2\max}}\right)^{3-D} \tag{1}$$

$$\log V_p = (3-D)\log(T_2) + (D-3)\log(T_{2\max}) \tag{2}$$

In the above Equations, Vp is the accumulative volume fraction (<T_2) (Zhou and Kang, 2016). T_{2max} are the maximum T_2 values, and they correspond to the largest pore sizes in NMR measurements. T_2 is the transverse relaxation time, and D is fractal dimension.

In Equation (2), the fractal dimension is hoped to be derived by taking the logarithm in both sides of the equation, since a straight line with a slope "D" will be obtained.

However, when presented logVp and logT_2 in the double-logarithm coordination, actually not a straight line but a smooth curve is encountered (Fig. 3B) (Lai et al., 2018, 2019). Therefore it should be noted that the fractal model which uses NMR tests to calculate fractal dimensions can be applied in high permeability (>100 mD) sandstones (Wang et al., 2018). For tight sandstone, low porosity dolostone or oil shale reservoirs, the fractal model becomes limited due to tortuous pore assemblage and complex poor structure (Lai et al., 2018, 2019).

Consequently a new model is derived by Lai et al. (2018), in which

$$\log\left(N\left(r_j\right)\right) + \log A = -D\log B - D\log\left(T_{2i}\right) \tag{3}$$

In Eq. (3), $j = i+1$; T_{2i} is the ith T_2 value, $N(r_j)$ are the numbers of pores with radius larger than r_i (characteristic pore size at the corresponding T_{2i}), $A = \frac{1}{36\pi\rho^3}$, and $B = 3\rho$, ρ is the surface relaxivity.

By plotting log($N(r_j)$ against log(T_2) for the same NMR T_2 spectrum, a straight line with a coefficient of determination (R^2) over 0.97 is observed (Fig. 3C). The fractal dimension is determined as 2.7598 from the slope of the line (Fig. 3C).

2.2. Experimental measurements

Core-measured porosity and permeability were obtained from core plug samples (1 inch in diameter) using a CMS-300 instrument at the State Key Laboratory of Petroleum Resources and Prospecting, China University of Petroleum (Beijing). Thin sections were impregnated with blue epoxy samples to highlight porosity. Carbon was coated on freshly broken core plug samples for Scanning Electron Microscope (SEM) analysis, in order to identify the various types of clay minerals and related micropores. SEM was also performed at State Key Laboratory of Petroleum Resources and Prospecting. NMR tests were performed on core plug samples to determine pore size distributions. The NMR T_2 distributions were measured at 20 °C using a 2 MHz Suzhou Niumag Analytical Instrument at State Key Laboratory of Petroleum Resources and Prospecting. The waiting time of NMR apparatus is 6000 ms, and the echo spacing (Te) is 0.12 ms, and 64 stacks were performed to derive relaxation curves. The samples were firstly fully (100%) saturated with brine, and the incremental and cumulative T_2 distributions were measured. Then the samples were removed with movable brine by a centrifugal machine with a rotation speed of 6000r/min. Then the T_2 distributions at centrifugal status were also obtained. Actually, typical T_2 spectra include both the incremental and cumulative T_2 distributions at the saturated and centrifugal status (Fig.2; Fig.3A) (Wang et al., 2018).

In NMR T_2 spectra, the water content (pore volume) is proportional to signal amplitude porosity (Dillinger and Esteban L., 2014; Wang et al., 2018). Small T_2 components (T_{2s}) in T_2 spectra refer to small pores (large surface-to volume ratio), whereas large T_2 components (T_{2l}) correspond to large pores (small surface-to-volume ratio) (Mü;ller--Huber et al., 2016; Lai et al., 2016; Lai et al., 2020). Mobile fluids commonly exhibit long T_2 components, while irreducible fluids produce short T_2 values due to the restriction of molecular motion in small pores (Mitchell and Fordham, 2014; Dillinger and Esteban L., 2014; Meng et al., 2016; Wang et al., 2018; Wang et al., 2020). Besides NMR porosity, NMR spectra can be used to derive NMR parameters such as Bulk Volume of Immovable fluid (BVI), Free Fluid Index (FFI) and T_{2gm} (amplitude weighted mean on a logarithmic scale) (Pape and Clauser, 2009; Meng et al., 2016; Wang et al., 2018).

3. Results

3.1. Pore spaces and oil bearing property

The Funing oil shale reservoirs in Subei Basin have a narrow porosity range from 0.18% to 7.82% (av. 2.14%), while permeability has a wide range from 0.000002 to 11.73 mD (av. 0.13 mD) (Liu et al., 2020). The complex porosity-permeability relationship implies a heterogeneous pore throat assemblage and a complex pore network.

SEM images reveal that the pore spaces include micro-fractures (Fig. 4A), organic-matter pores (Fig. 4B), (primary) interparticle pores (Fig. 4C–D), (secondary) intragranular dissolution pores (Fig. 4E–F), and micropores associated with authigenic clay minerals (Fig. 4G), as well as minor intercrystal pores within pyrite crystals (Fig. 4H). These pore spaces, which are abundant in oil shale reservoirs, are commonly below the resolution limit of optical microscope (thin sections), but can be

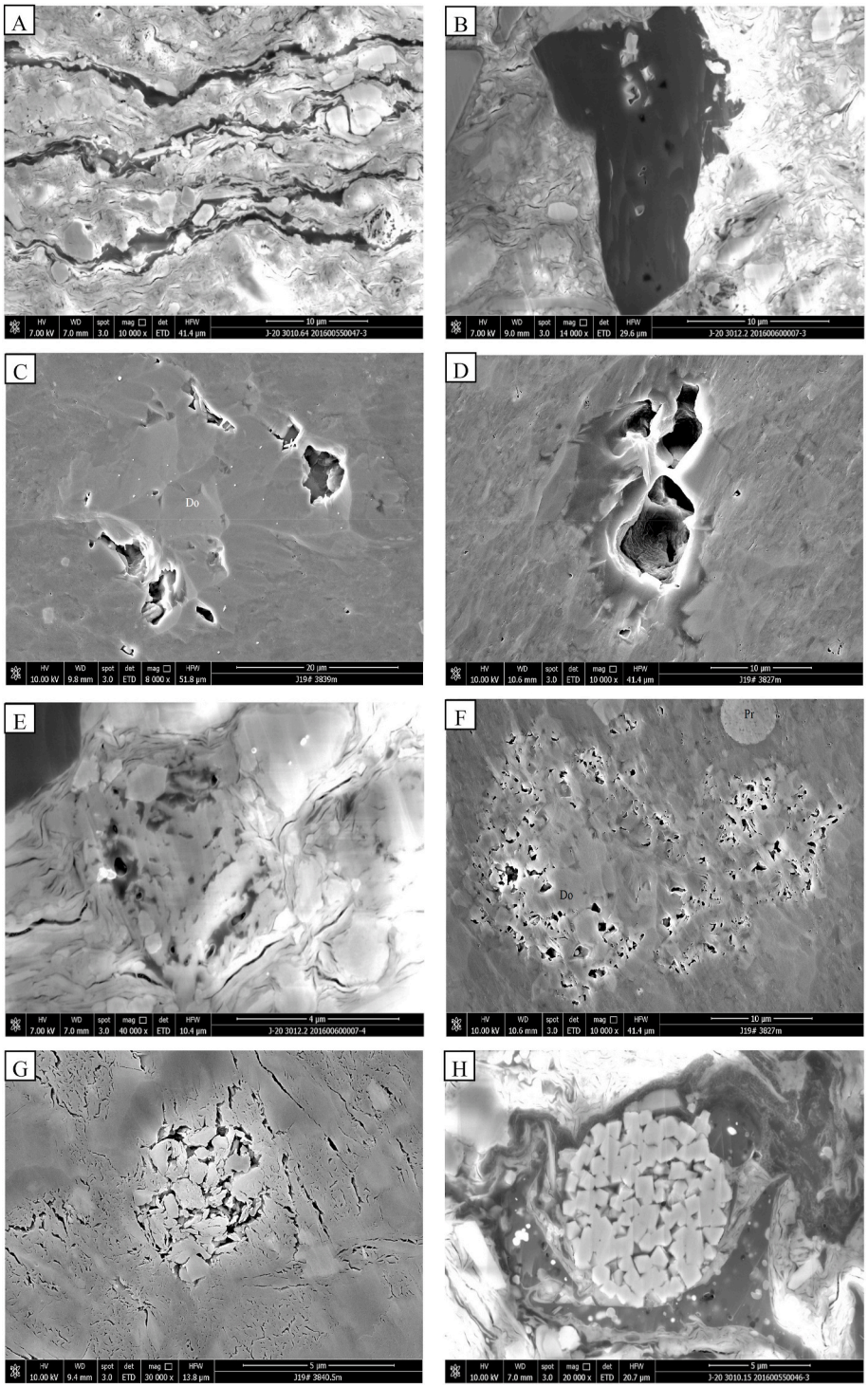

Fig. 4. Various pore spaces revealed by SEM images in oil shales of Funing Formation in Subei Basin. A. Micro-fractures containing organic matters, J20, 3010.64 m. B. Organic-matter pores, J20, 3012.2 m. C. Primary interparticle pores, J19, 3839 m. D. Primary interparticle pores, J19, 3827 m. E. Secondary intragranular dissolution pores, J-20, 3012.2 m. F. Intragranular dissolution pores. G. Micro-porous (intercrystal pores) clay minerals associated with dissolved grains, Ji19 3840.5 m. H. Strawberry-like pyrite crystals abundant with intercrystal pores, J20, 3010.15 m.

detected by SEM (BSE) analysis (Loucks et al., 2009, 2012; Zhang et al., 2018).

Additionally fluorescence thin sections indicate that micro-fractures (Fig. 5A-B), interparticle pores (Fig. 5C-D), intragranular dissolution pores (Fig. 5E-F) are hydrocarbon bearing since they emit strong dark blue fluorescences (Fig. 5A-E). Conversely clay minerals (detrital clay or authigenic clay minerals), appearing as layers or nodules in fluorescence thin sections, commonly lack fluorescence or emit weak scattered fluorescence (Fig. 5G-H). Additionally, organic matters, which are recognized as dark regions in fluorescence thin sections, are fluorescence free, however, oil can exist in organic matter pores since scattered fluorescence can be observed (Fig. 5I-J). Almost all the pore realms ranging from organic matter pores to interparticle pores are oil bearing in the Funing Formation.

3.2. NMR T_2 spectra and fractal analysis

The NMR T_2 spectra, which measure interactions between pore fluids and grain surfaces, contain abundant information about pore (body) size distribution (Dillinger and Esteban, 2014; Wang et al., 2018; Lai et al., 2019). In theory, pore bodies with large size have longer (large) T_2 values, while T_2 relaxation times of small pore bodies are short/small

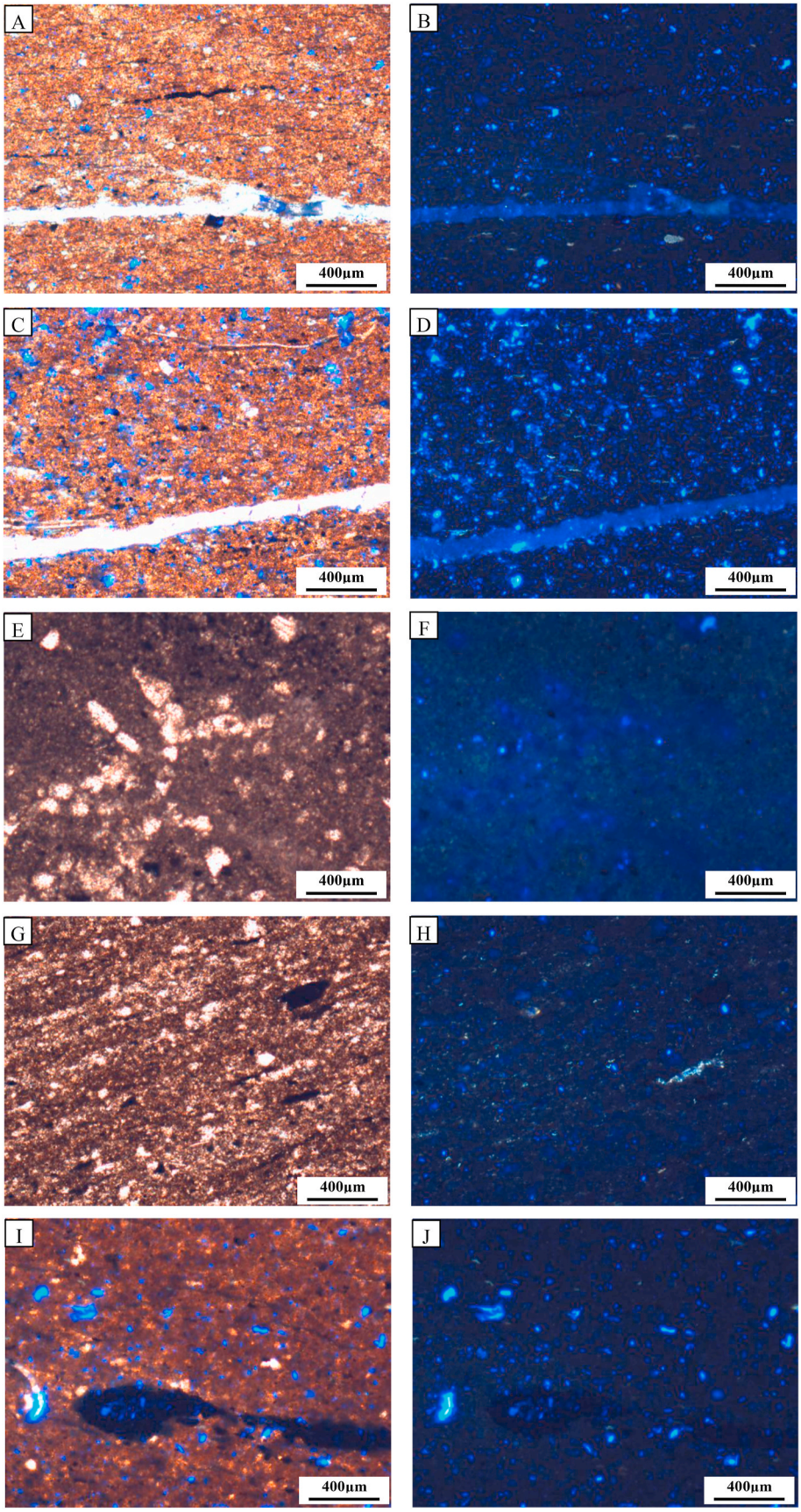

Fig. 5. Fluorescence thin sections under plane polarized light and fluorescence light to show fluorescence characteristics of various pore spaces in oil shales of Funing Formation in Subei Basin. A. Filled micro-fractures, Ji19, 3811.44 m. B. Micro-fracture displays dark blue fluorescence, the same field view of A. C. Quartz and dolomite particles, and filled micro-fracture, Ji 19, 3828.5 m. D. The edges of particle emits weak blue fluorescence, indicating the interparticle pores are oil bearing, the same field view of B. E. Feldspar and carbonate particles, 3896.25 m. F. Intraparticle dissolved pores emit scattered blue fluorescence, the same field view of E. G. Abundant detrital clay (layered), the particles are mainly carbonates, 3900.5 m. H. The detrital clays are fluorescent free, and some intraparticle areas emit dark blue fluorescence, the same field view of G. I. Dark areas are organic matters, Ji19, 3814.34 m. J. Organic matter pores emit blue fluorescence, the same field view of I.. (For interpretation of the references to colour in this figure legend, the reader is referred to the Web version of this article.)

(Rezaee et al., 2012; Dillinger and Esteban, 2014; Müller-Huber et al., 2016; Meng et al., 2016; Wang et al., 2018; Lai et al., 2020). In addition, in NMR T_2 spectra, the higher the signal amplitude at certain T_2 values, the more the fluid at this pore sizes (T_2 value) will be (Pape and Clauser, 2009; Meng et al., 2016; Zhang et al., 2020). Therefore the fluid content encountered at certain pore sizes can be calculated according to cumulative T_2 distribution (Meng et al., 2016).

In this sub-section, NMR T_2 spectra or pore size distribution characteristics of both saturated and centrifugal status are presented. Then NMR T_2 spectra of both saturated and centrifugal status are used for fractal analysis to quantitatively characterize the complexity of the pore structures of Funing oil shale reservoirs (Fig. 6; Fig. 7).

3.2.1. NMR T_2 spectra

Typical NMR T_2 spectra of Funing oil shales are presented in Fig. 2, 3A and 6 and 7, and the cumulative porosity distributions as a function of T_2 are also presented. The T_2 spectra of these four samples mainly display bi-modal behaviors and left skewed (low right peak but high left peak) (Fig.2; Fig.3; Fig.6; Fig.7). Commonly the signal amplitudes of T_2 components larger than 10 ms are very low, and there are very weak T_2 components less than 0.1 ms.

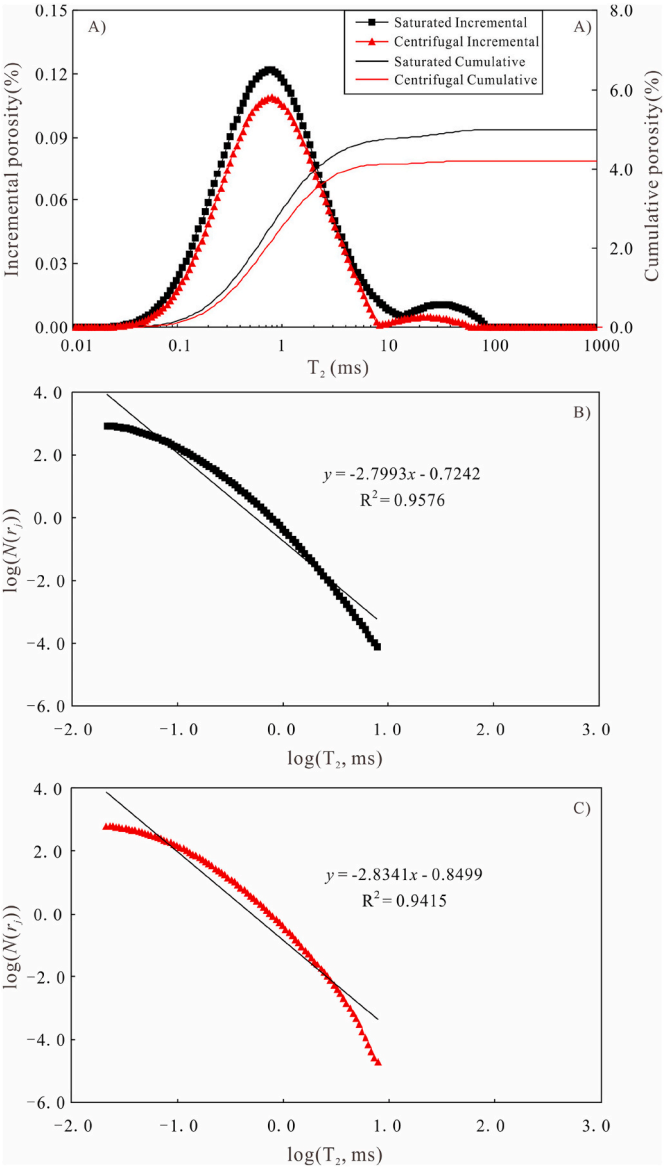

Fig. 6. NMR T_2 spectra and related fractal dimension calculation at saturated and centrifugal status in oil shales of Funing Formation in Subei Basin.

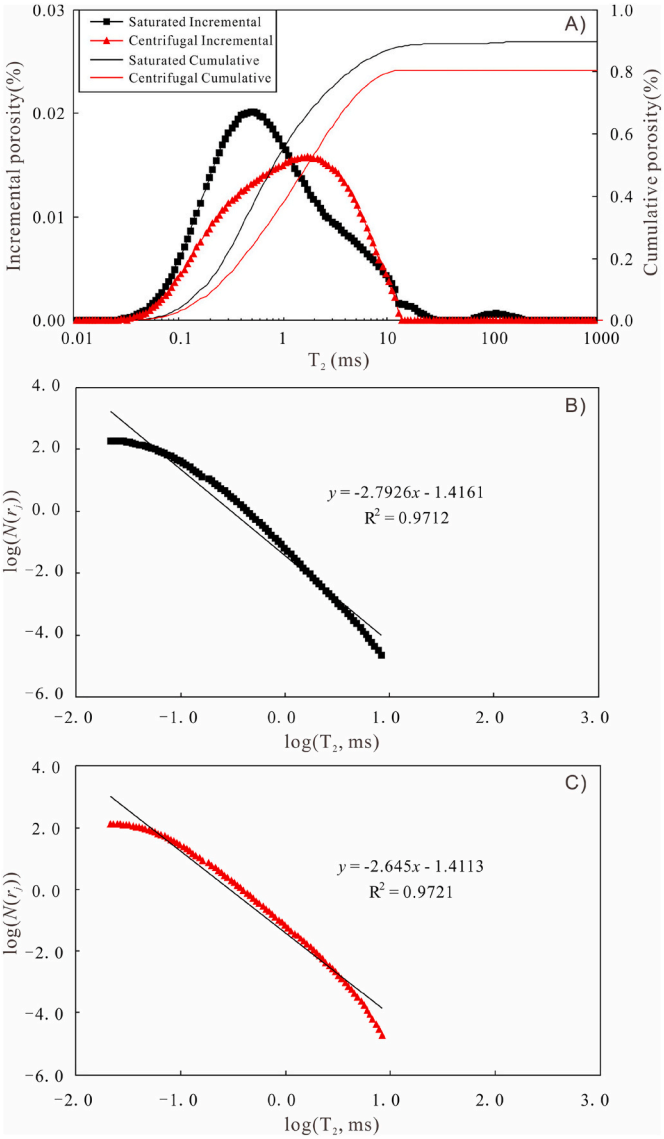

Fig. 7. NMR T_2 spectra and related fractal model to calculate fractal dimension at saturated and centrifugal status in oil shales of Funing Formation in Subei Basin.

The main peaks disappear at about 0.1–10 ms, and the cumulative porosity distributions reach their maximum values at about 10 ms. From the T_2 spectra of these four samples, most of the T_2 components are short (<10 ms), and there are tiny tail distribution with T_2 component larger than 10 ms. Actually T_2 spectra for most of the samples appear at T_2 ranges from 0.1 to 10 ms (Fig.2; Fig.3; Fig.6; Fig.7). The two distinct peaks imply discontinuous pore size distributions (Lai et al., 2018). The small pore realms (intraparticle (matrix) pores, micropores) are related to left peak, while the large pore realms including micro-fractures as well as the interparticle pores correspond to right peaks (Liu et al., 2020) (Fig.2; Fig.3; Fig.6; Fig.7). This is in accordance with pore systems by SEM analysis (dominant intragranular pores and micropores, minor amounts of large interparticle pores, and occasionally microfractures are observed) (Fig. 4A–H). However, there are also minor samples displaying unimodal T_2 behaviors (only one modal is presented, no right peak, and no tail distribution), possibly implying a continuous range of pore size (good sorting of the pore systems). Also, the samples with unimodal T_2 distributions contain only small pore realms including intraparticle pores, clay mineral related micropores, organic matter

pores, while no micro-fractures or interparticle pores can be detected (Fig. 4A–B; 4 E-4F; Fig. 5E-F; 5G-5H).

NMR spectra measured at saturated and centrifugal status are different. However, in some samples, the saturated incremental and centrifugal incremental curves are not evidently deviated (Fig.2; Fig.6), indicating that only minor amounts of fluids are movable, and most of the fluids are irreducible due to poor pore connectivity. Actually, BVI values for some samples can reach as high as 90% (Liu et al., 2020). Conversely, there are some samples having relatively low content of irreducible fluid, and large amount fluids can be removed by the centrifugal machine. Consequently, the saturated incremental and centrifugal incremental curves can be significantly deviated (Fig.3; Fig.7), implying a low irreducible water content and favorable fluid mobility.

From NMR T_2 spectrum, parameters including T_{2gm} (amplitude weighted means on a logarithmic scale) and $T_{2cutoff}$, can be derived (Gao and Li, 2015). T_{2gm} represents both microscopic pore structure and macroscopic petrophysical properties (Lai et al., 2018), and the higher the T_{2gm} parameter, the better the reservoir quality will be (Wang et al., 2018). T_{2utoff} separates irreducible BVI (Bulk Volume of Immovable fluid) (T_2 components $< T_{2cutoff}$) and movable FFI (Free Fluid Index) ($>T_{2cutoff}$) (Zhang et al., 2018; Liu et al., 2020). Therefore, both irreducible fluid and movable fluid content can be determined given that $T_{2cutoff}$ is known from T_2 spectrum.

3.2.2. *Fractal dimension calculation*

Eq. (3) foresees that the relationship between $N(r_j)$ and T_2 is linear on a log–log plot. Log ($N(r_j)$)-log(T_2) plots at saturated and centrifugal status were constructed respectively for all the samples (Figs. 6 and 7). Straight lines with evident slope are observed, and the best fitting lines can be obtained through regression analysis. The results reveal that all of the plots show good fits (correlation coefficients >0.9), indicating that the Funing oil shales are fractal and can be described by the fractal model in Eq. (3). Then the fractal dimensions can be derived from the slope of the best fit lines, for instance, the slopes of the log ($N(r_j)$)-log(T_2) plots in Fig. 6B (fractal analysis performed on T_2 spectrum at saturated status) give the fractal dimensions of February 2, 7993, while the slope of best fitting line in Fig. 6C (fractal analysis performed on T_2 spectrum at centrifugal status) gives a fractal dimension of 2.8341 (Fig. 6). The accuracy of the fractal model can be evaluated by the coefficient of determination (Sakhaee-Pour and Li, 2016), and the high values of R^2 indicate that it is sufficient to use the fractal models for the fractal dimension calculation (Figs. 6 and 7).

The calculated fractal dimensions (Ds) are in the range from 2.566 to 2.887 with an average of 2.715 for T_2 spectrum at saturated status, while calculated fractal dimensions (Dc) for T_2 spectrum at centrifugal status range from 2.623 to 2.905, and averaged as 2.781. Therefore the fractal behavior of oil shales reveal a signature of a volume fractal since the calculated fractal dimensions are in the range from 2.0 to 3.0, which is in accordance with the fractal dimensions of three-dimensional pore spaces (Cai et al., 2010; Giri et al., 2012; Gao et al., 2014; Wang et al., 2018; Zhang et al., 2020).

It should be noted that not all the pore systems can be characterized by the fractal model. As can be seen from the fractal curve, the tail distributions ($T_2 > 10$ ms) can't be scaled with the fractal curves (Figs. 6 and 7). Actually, the longest T_2 components (>10 ms or larger) are off the straight fitting lines, and therefore are not fractal with the entire pore realms. Besides the very minor amounts of large T_2 components, almost the T_2 components ranging from 0.01 ms to about 10 ms can be described by the fractal model (Figs. 6 and 7).

4. Discussion

NMR T_2 spectrum is used for characterizing pore size distribution, and pore bodies as small as 3 nm can be detected by NMR tests (Gao and Li, 2016; Xiao et al., 2016). While SEM analysis is used for analyzing the morphology and quantity of various pore spaces. The interparticle pores, micro-fractures are suggested to significantly contribute to fluid mobility, resulting in a lowest BVI value (Liu et al., 2020). Particle (dolomite and feldspar) dissolution pores and intercrystal pores have irregular and jagged morphologies, and are not always connected by effective throats. Therefore, they are not effectively movable, resulting in moderate BVI values. Organic pores and clay mineral micro-pores have poor connectivity, and resulting in the highest BVI values. Therefore the coexistence of micro-fractures, particle (dolomite and feldspar) dissolution pores and intercrystal pores as well as organic pores contribute to the uni-modal, bimodal or continuous, discontinuous pore size distribution determined from NMR T_2 spectra (Fig.2; Fig.3; Fig.6; Fig.7). Samples containing large pore realms ($T_2 > 10$ ms or tail distribution) generally have low BVI values due to the presence of micro-fractures or interparticle pores. Conversely, high content of irreducible fluid will be encountered if the T_2 components are mainly short ($T_2 < 10$ ms) since the abundance of short T_2 components imply the dominance of intercrystal pores as well as organic pores (Fig.2; Fig.3; Fig.6; Fig.7).

Crossplots of BVI versus porosity and permeability show that the high BVI values are commonly associated with low permeability, indicating the connectivity of pore systems determines fluid mobility (Fig. 8). However, BVI values show complex relationships with porosity, indicating that it is not pore volume determining fluid mobility, but the pore connectivity (Liu et al., 2020) (Fig. 8).

Reservoir quality index (*RQI*), defined as the ratio of permeability (μm^2) to fractional porosity under the square root (Eq. (4); Amaefule et al., 1993; Lai et al., 2016; Tavakoli et al., 2011). RQI is widely used for addressing reservoir quality in various scales, and it links microscopic pore structure with macroscopic reservoir quality (Lai et al., 2015; Zhao

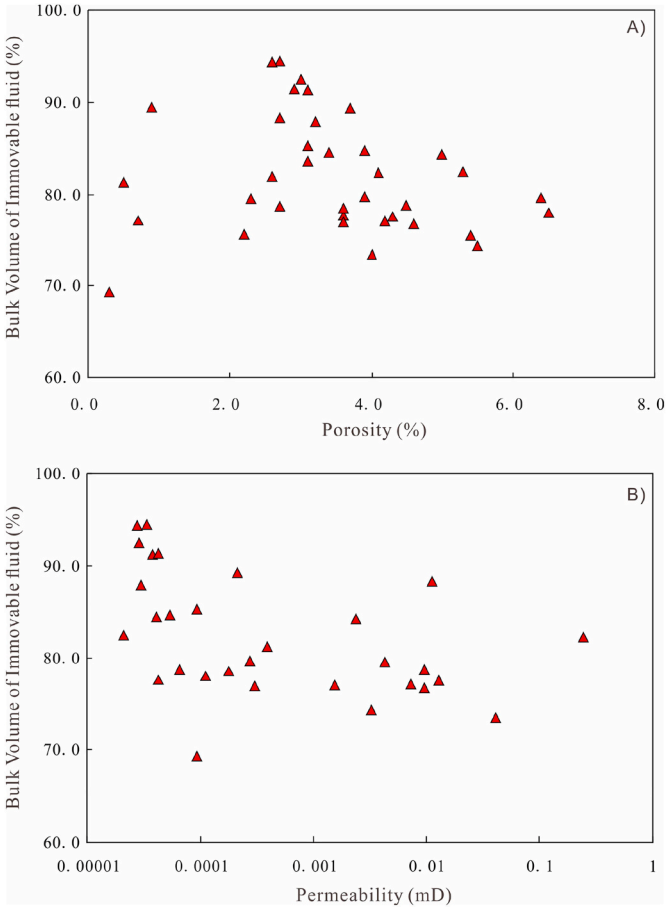

Fig. 8. Crossplots of NMR BVI (Bulk Volume of Immovable fluid) versus porosity and permeability in oil shales of Funing Formation in Subei Basin.

et al., 2017a,b,c).

$$RQI = \sqrt{\frac{K}{\varphi}} \quad (4)$$

However, regression analysis reveals that RQI fails to correlate with $T_{2cutoff}$ and BVI values (Fig. 9). However, NMR can be linked with each other, for instance, $T_{2cutoff}$ shows relatively strong correlation with BVI, and $T_{2cutoff}$ is higher in samples with high BVI values (Fig. 10). Therefore, the Funing oil shale shows a complex pore network from the aspects of NMR pore size distribution (Liu et al., 2020), and fractal dimensions need to be calculated to characterize the complexity of pore structure in oil shales.

In this subsection, the fractal behaviors of T_2 spectrum measured at saturated and centrifugal status (movable and irreducible pore realms) are analyzed respectively.

4.1. Fractal behaviors of T_2 spectra at saturated and centrifugal status

For the entire T_2 ranges (0.1–10 ms, or even larger), the crossover and overlap of the two spectra (saturated and centrifugal status) can be detected, implying that large pore bodies may also be isolated and not connected by effective throats (Fig.2; Fig.3; Fig.6; Fig.7). Additionally, the full signal amplitudes, i.e., the total NMR porosity measured at saturated and centrifugal status are not deviated evidently, indicating that most of pore volumes are irreducible (Fig.2; Fig.3; Fig.6; Fig.7). Actually, BVI ranges from 69.3% to 94.5% with an average of 82.03% (Fig.8; Fig.9).

Fractal analysis was performed on the two spectra measured at

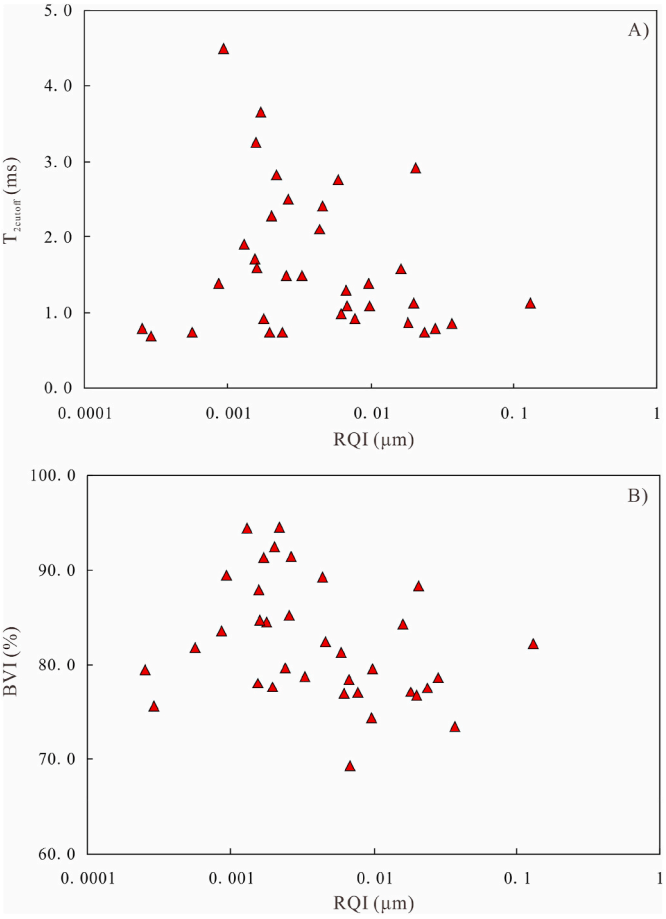

Fig. 9. Crossplots of NMR $T_{2cutoff}$ and BVI (Bulk Volume of Immovable fluid) versus RQI in oil shales of Funing Formation in Subei Basin.

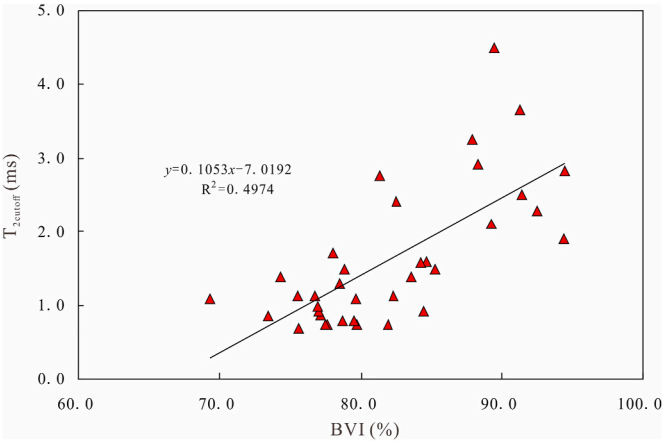

Fig. 10. Crossplots of NMR $T_{2cutoff}$ versus BVI (Bulk Volume of Immovable fluid) in oil shales of Funing Formation in Subei Basin.

saturated and centrifugal status respectively for all the 36 samples according to Eq. (3). Then fractal dimension (Ds) for T_2 spectrum at saturated status and fractal dimension (Dc) at centrifugal status are calculated, respectively. The two fractal dimensions are in the range from 2.5 to 2.9, implying a complex pore assemblage. Fig. 11 exhibits the fractal dimension calculated at saturated status plotted against fractal dimension at centrifugal status. Fractal dimensions (Dc) for centrifugal T_2 spectra are generally higher than those for saturated T_2 spectra. Most of the data points lie below the y = x line in the crossplot of fractal dimension (Dc) versus fractal dimension (Ds) (Fig. 11). Therefore the irreducible pore realms (centrifugal T_2 spectra) display more complexity than the saturated T_2 spectra (entire pore realms) (Fig. 11). As we know, NMR could characterize pores spanning over a wider range (tens of nanometers to several hundred microns) (Xiao et al., 2016). More small pores are associated with T_2 spectrum at centrifugal status. Micropores (associated with centrifugal T_2 spectra) actually have a great impact on fractal dimension and thus complexity of pore structure, and therefore fractal dimensions are higher for centrifugal T_2 spectra (Lai and Wang, 2015; Wang et al., 2018).

Regression analysis between NMR parameters and the two fractal dimensions show that fractal dimensions (Dc) for centrifugal T_2 spectra are strongly negatively correlated with BVI values (Fig. 12). High fractal dimension values correspond to low BVI values (Fig. 12). Fractal dimensions (Ds) for saturated T_2 spectra have no evident correlation relationships between BVI (Fig. 12). Additionally, $T_{2cutoff}$ parameter also displays no evident relationship with fractal dimensions (Ds) (Fig. 13),

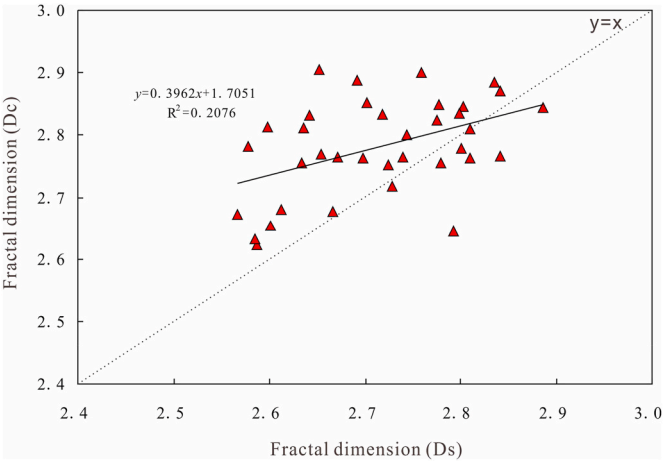

Fig. 11. Correlation between fractal dimensions calculated from T_2 spectra at saturated status (Ds) and centrifugal status (Dc), respectively.

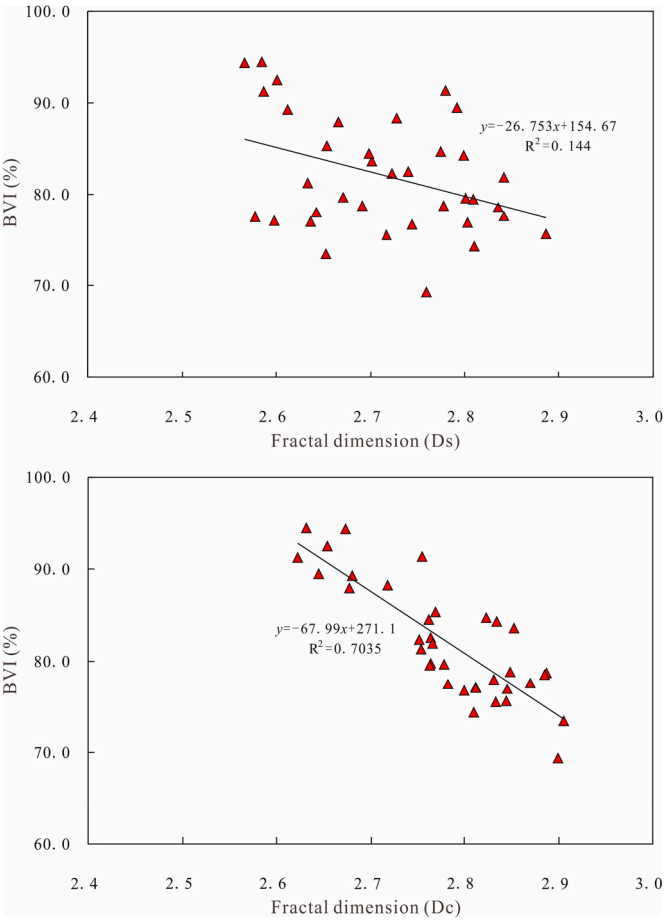

Fig. 12. Crossplots of BVI versus fractal dimensions (Ds) and (Dc) in oil shales of Funing Formation in Subei Basin.

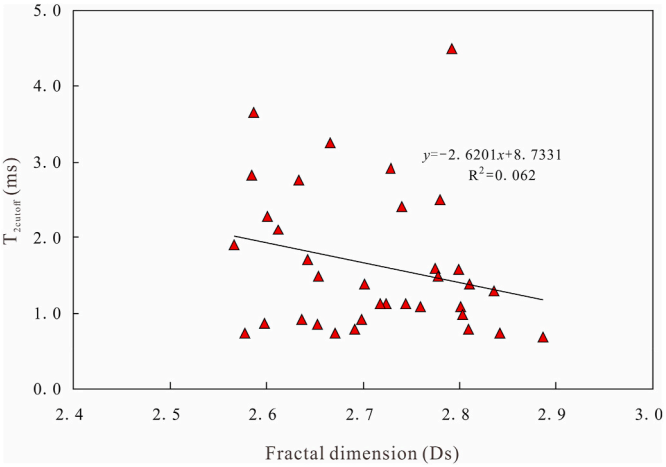

Fig. 13. Crossplot of NMR $T_{2cutoff}$ versus fractal dimension (Ds) calculated from T_2 spectra at saturated status.

but strongly negative correlation with fractal dimensions (Dc) for centrifugal T_2 spectra (Fig. 14). Consequently, fractal dimensions for centrifugal T_2 spectra, which represent the complexity of irreducible pore realms, can reflect the NMR parameters. The content of T_2 components (<1 ms) determines the fluid mobility in the Funing oil shale reservoirs in the Subei Basin, and high content of short T_2 components will result in high BVI values (Liu et al., 2020) (Fig. 12). The linear trendline with a regression coefficient $R^2 > 0.7$ supports a strong positive relationship

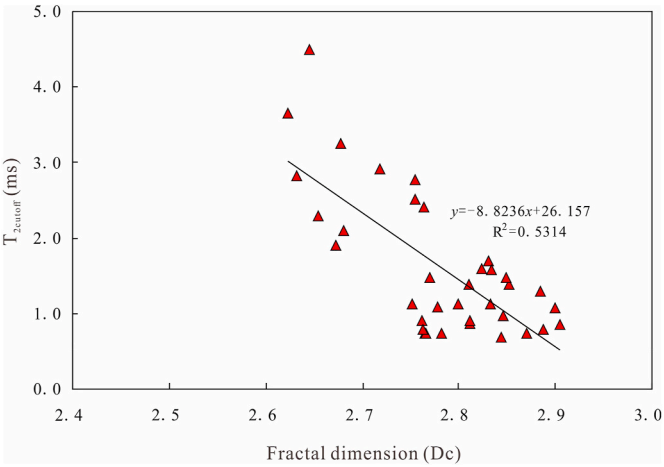

Fig. 14. Crossplot of NMR $T_{2cutoff}$ versus fractal dimension (Dc) calculated from T_2 spectra at centrifugal status.

between BVI and the fractal dimensions (Fig. 12). Conversely, fractal dimension (Ds) for T_2 spectra at saturated status fail to reflect the macroscopic NMR behaviors.

4.2. *Implication for pore structure evaluation*

Fractal theory offers a quantitative description of complexity of reservoir rocks (Daigle et al., 2014b; Wang et al., 2018; Zhang et al., 2020). Fractal dimensions are representations of rock heterogeneity, and allows to express the shapes of pores and pore channels as a quantitative number (Lesniak Such, 2005; Gao and Li, 2015; Wang et al., 2018). Commonly the higher the fractal dimensions, the more complexity and heterogeneous of pore structure will be (Li and Horne, 2006).

As can be seen from Figs. 12 and 14, high fractal dimension values are associated with low BVI and low $T_{2cutoff}$ values (Fig.12; Fig.14). Therefore the high fractal dimensions for centrifugal T_2 spectra, which represent more complexity of irreducible pore realms, are related to low BVI and $T_{2cutoff}$ values (Fig.12; Fig.14). Additionally, fractal dimensions for saturated T_2 spectra have complex relationships between BVI values (Fig.12; Fig.14). Though fractal dimensions for centrifugal T_2 spectra can reflect the macroscopic NMR behaviors, the centrifugal T_2 spectra can't take the large T_2 components (>10 ms) and T_2 tail distributions into consideration since these data point are off the straight lines (Fig.6; Fig.7).

In fractal analysis, there are some large T_2 components (>10 ms or even larger) off the straight fitting lines, and therefore they are not self-similar with the entire pore realms. On the one hand, larger pore realms (interparticle pores and micro-fractures) in shale oil reservoirs, cannot be described by the same fractal dimension with small pore realms (intragranular pores, clay mineral micro-pores and organic matter pores). On the other hand, diffusion relaxation must be considered in rocks with large pore realms (Daigle et al., 2014a). Therefore, the large pore realm associated with T_2 components>10 ms may not be self-similar with the dominant pore spaces (intragranular pores, clay mineral micro-pores and organic matter pores) in oil shales, and can't be described using the fractal models in Eq. (3).

Samples with low BVI values, which are suggested to have good reservoir quality, tend to have high fractal dimensions and high complexity degree of pore structures (Figs. 12 and 14). The coexistence of interparticle pores and micro-fractures results in a high complexity degree of pore structure and therefore high fractal dimension. On the contrary, fractal dimensions will be lower if one type of pores (small pore realms) dominates the pore spaces.

Though there are minor amounts of large T_2 components (tail T_2

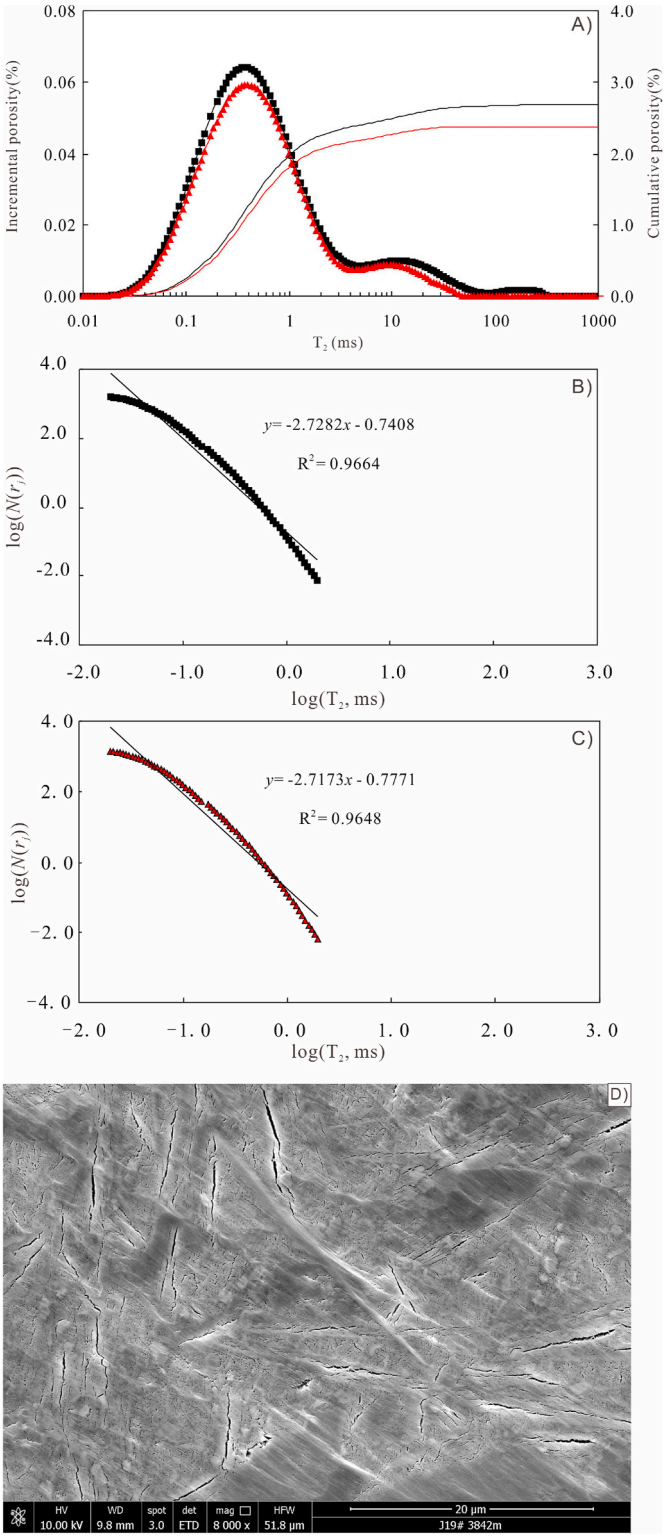

Fig. 15. Typical NMR T_2 spectrum and fractal behaviors at saturated and centrifugal status as well as pore spaces in oil shales of Funing Formation in Subei Basin.

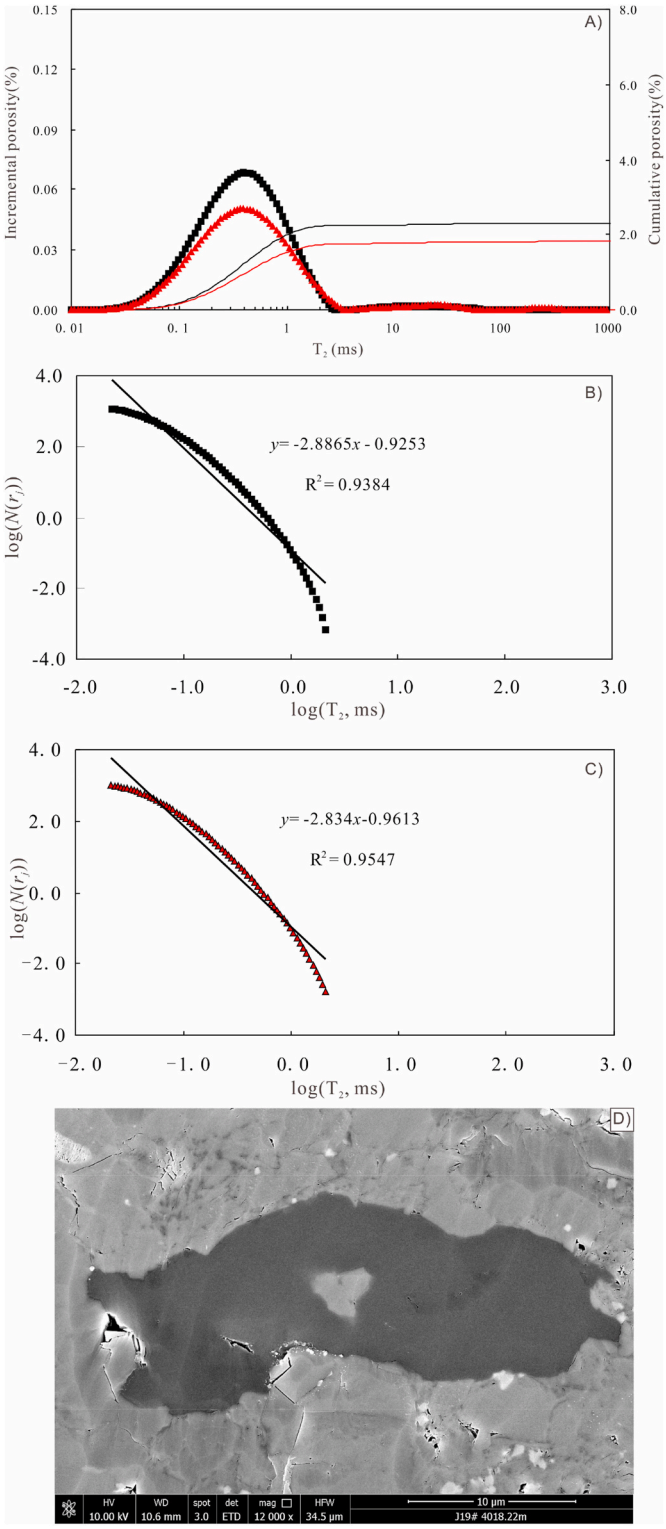

Fig. 16. NMR T_2 spectrum and fractal behaviors at saturated and centrifugal status as well as pore spaces in oil shales of Funing Formation in Subei Basin.

distribution), they make a significant contribution to permeability since micro-fractures and interparticle pores have large aperture, and are important for fluid flow in oil shale reservoirs (Liu et al., 2020). Samples with the best reservoir quality commonly have long T_2 components or even tail distributions, which are associated with interparticle pore of micro-fractures (Liu et al., 2020). However, these long T_2 components (>10 ms) and tail distributions, generally can't be treated as an integral pore system with the irreducible pore realms, therefore resulting in the complex relationships between calculated fractal dimensions and NMR parameters.

Presented in Fig. 15 is a bi-modal T_2 spectrum with tail distributions, and SEM analysis confirm the presence of microfractures, which refer to the right T_2 peaks. The calculated fractal dimensions for saturated and

centrifugal T_2 spectra are 2.7282 and 2.7173 respectively (Fig. 15). The uni-modal T_2 distribution without tail distributions is displayed in Fig. 16, and the signal amplitudes reveal a poor reservoir quality but high BVI values. The calculated fractal dimensions for saturated and centrifugal T_2 spectra are 2.8865 and 2.834, respectively (Fig. 16). From Figs. 15 and 16, it can be concluded that samples with bi-modal T_2 distributions (containing tail distribution and large T_2 components) generally have low fractal dimensions since the large T_2 components and tail distributions are not self-similar with the entire pore systems, and therefore are not fractal. On the contrary, the samples with uni-modal T_2 distributions (no tail distribution or large T_2 components) have high fractal dimensions since the coexistence of various pore spaces will result in a complexity and heterogeneous pore assemblage (Figs. 15 and 16).

The different fractal behaviors of T_2 spectrum at saturated and centrifugal status reflect the pore assemblage of organic matter pores, intragranular dissolution pores, intercrystal micropores, interparticle pores and microfractures (Figs. 15 and 16). The small pore realms, including organic matter pores, intragranular dissolution pores, intercrystal micropores, which are associated with centrifugal T_2 spectrum, determine the microscopic heterogeneity and complexity. The large pore realms, which include interparticle pores and micro-fractures, are associated with the long T_2 components and tail distribution of saturated T_2 spectrum, and they control the macroscopic reservoir quality of oil shales. Fractal behaviors varied between saturated and centrifugal T_2 spectrum, and fractal dimensions on the one hand describe complexity of pore throat structure, on the other hand they characterize the macroscopic behaviors of reservoir rocks (Wang et al., 2018). Fractal analysis gives important insights in the heterogeneous assemblage of pore systems, and can help quantitatively describe complexity of pore structure.

5. Conclusions

The oil shales of Funing Formation in Subei Basin have various pore spaces including organic matter pores, intragranular dissolution pores, intercrystal micropores, interparticle pores and microfractures. The NMR T_2 pore size distributions are mostly bimodal (left-skewed) due to abundance in small pore realms. The right peak or tail distribution mainly corresponds to large pore realms (interparticle pores and microfractures). NMR parameter BVI shows good correlations with $T_{2cutoff}$.

Fractal analysis was performed on the NMR T_2 spectra measured at saturated and centrifugal status, respectively. Fractal dimensions calculated from T_2 spectrum at centrifugal status are higher than those at saturated status. Fractal dimensions calculated from T_2 spectrum at centrifugal status show negatively correlation relationships with BVI and $T_{2cutoff}$ values. The different fractal behaviors of T_2 spectrum at saturated and centrifugal status reflect the complex pore assemblage in oil shales.

The small pore realms (organic matter pores, intragranular dissolution pores, intercrystal micropores) determine the microscopic heterogeneity and complexity. The large pore realms (interparticle pores and micro-fractures) control the macroscopic reservoir quality of oil shales. However they are not self-similar with the small pore realms, and can't be described with the fractal dimension. Fractal analysis can give insights in the heterogeneous assemblage of pore systems and help describe complexity of pore structure.

Author contribution statement

Xiaoping Liu: Conceptualization, Methodology, Software, Data curation, Writing – original draft, Writing- Reviewing and Editing; Zhijun Jin: Conceptualization, Methodology, Software; Jin Lai: Conceptualization, Methodology, Software, Data curation, Writing – original draft, Writing- Reviewing and Editing; Xuechun Fan.: Data curation, Writing – original draft; Ming Guan: Visualization, Investigation, Software, Validation, Writing- Reviewing and Editing; Honglin Shu: Visualization, Investigation; Gaocheng Wang: Visualization, Investigation; Mengcai Liu: Writing- Reviewing and Editing; Yufeng Luo: Writing- Reviewing and Editing

Declaration of competing interest

The authors declare that they have no known competing financial interests or personal relationships that could have appeared to influence the work reported in this paper.

Acknowledgments

We thank PetroChina Zhejiang Oilfield Company for providing samples and data access. This work was financially supported by the National Natural Science Foundation of China (Grant No. 42072150, 41372144) and the National Science & Technology Major Project of China (Grant No. 2017ZX05049-001-008) and, and we thank the sponsors of these projects.

Appendix A. Supplementary data

Supplementary data to this article can be found online at https://doi.org/10.1016/j.marpetgeo.2021.105069.

References

Amaefule, J.O., Mehmet, A., Djebbar, T., David, K., Dare, K., 1993. Enhanced reservoir description: using core and log data to identify hydraulic (flow) unit and predict permeability in uncored intervals/well. In: SPE26436, Presented at the 68th Annual SPE Conference and Exhibition, Houston, Texas, 1993.

Anovitz, L.M., Cole, D.R., Rother, G., Allard, L.F., Jackson, A.J., Littrell, K.C., 2013. Diagenetic changes in macro- to nano-scale porosity in the St. Peter Sandstone: an (ultra) small angle neutron scattering and backscattered electron imaging analysis. Geochem. Cosmochim. Acta 102, 280–305.

Cai, J., Yu, B., Zou, M., Mei, M., 2010. Fractal analysis of invasion depth of extraneous fluids in porous media. Chem. Eng. Sci. 65, 5178–5186.

Cai, J., Wei, W., Hu, X., Liu, R., Wang, J., 2017. Fractal characterization of dynamic fracture network extension in porous media. Fractals - Complex Geometry, Patterns, Scaling Nat. Soc. 25 (2), 1750023.

Cheng, Q., Zhang, M., Li, H., 2019. Anomalous distribution of steranes in deep lacustrine facies low maturity source rocks and oil of Funing formation in Subei Basin. J. Petrol. Sci. Eng. 181, 106–190.

Curtis, M.E., Cardott, B.J., Sondergeld, C.H., Rai, C.S., 2012. Development of organic porosity in the Woodford Shale with increasing thermal maturity. Int. J. Coal Geol. 103, 26–31.

Daigle, H., Johnson, A., 2016. Combining mercury intrusion and nuclear magnetic resonance measurements using percolation theory. Transport Porous Media 111, 669–679.

Daigle, H., Thomas, B., Rowe, H., Nieto, M., 2014a. Nuclear magnetic resonance characterization of shallow marine sediments from the nankai trough, integrated ocean drilling program expedition 333. J. Geophys. Res. 119, 2631–2650. https://doi.org/10.1002/2013JB010784.

Daigle, H., Johnson, A., Thomas, B., 2014b. Determining fractal dimension from nuclear magnetic resonance data in rocks with internal magnetic field gradients. Geophysics 79 (6), D425–D431.

Dillinger, A., Esteban, L., 2014. Experimental evaluation of reservoir quality in Mesozoic formations of the Perth Basin (Western Australia) by using a laboratory low field Nuclear Magnetic Resonance. Mar. Petrol. Geol. 57, 455–469.

Gao, H., Li, H.A., 2015. Pore structure characterization, permeability evaluation and enhanced gas recovery techniques of tight gas sandstones. J. Nat. Gas Sci. Eng. 28, 536–547.

Gao, H., Li, H.A., 2016. Pore structure characterization, permeability evaluation and enhanced gas recovery techniques of tight gas sandstones. J. Nat. Gas Sci. Eng. 28, 536–547.

Gao, H., Yu, B., Duan, Y., Fang, Q., 2014. Fractal analysis of dimensionless capillary pressure function. Int. J. Heat Mass Tran. 69, 26–33.

Giri, A., Tarafdar, S., Gouze, P., Dutta, T., 2012. Fractal pore structure of sedimentary rocks: simulation in 2-d using a relaxed bidisperse ballistic deposition model. J. Appl. Geophys. 87, 40–45.

Guan, M., Liu, X., Jin, Z., Lai, J., 2020. The heterogeneity of pore structure in lacustrine shales: insights from multifractal analysis using N2 adsorption and mercury intrusion. Mar. Petrol. Geol. 114, 104150.

Hu, Q., Ewing, R.P., Dultz, S., 2012. Low pore connectivity in natural rock. J. Contam. Hydrol. 133, 76–83.

Jin, Y., Song, H.B., Hu, B., Zhu, Y., Zheng, J., 2013. Lattice Boltzmann simulation of fluid flow through coal reservoir's fractal pore structure. Sci. China Earth Sci. 56, 1519–1530.
Kleinberg, R.L., Kenyon, W.E., Mitra, P.P., 1994. Mechanism of NMR relaxation of fluids in rock. J. Magn. Reson., Ser. A 108 (2), 206–214.
Kulesza, S., Bramowicz, M., 2014. A comparative study of correlation methods for determination offractal parameters in surface characterization. Appl. Surf. Sci. 293, 196–201.
Lesniak, G., Such, P., 2005. Fractal approach, analysis of images and diagenesis in pore space evaluation. Nat. Resour. Res. 14 (4), 317–324.
Lai, J., Wang, G., 2015. Fractal analysis of tight gas sandstones using High-Pressure Mercury Intrusion techniques. J. Nat. Gas Sci. Eng. 24, 185–196.
Lai, J., Wang, G., Chai, Y., Ran, Y., Zhang, X., 2015. Depositional and diagenetic controls on reservoir pore structure of tight gas sandstones: evidence from lower cretaceous bashijiqike Formation in kelasu thrust belts, kuqa depression in tarim basin of west China. Resour. Geol. 65 (2), 55–75.
Lai, J., Wang, G., Fan, Z., Chen, J., Wang, S., Zhou, Z., Fan, X., 2016. Insight into the pore structure of tight sandstones using NMR and HPMI measurements. Energy Fuels 30, 10200–10214.
Lai, J., Wang, G., Fan, Z., Zhou, Z., Chen, J., Wang, S., 2018. Fractal analysis of tight shaly sandstones using nuclear magnetic resonance measurements. AAPG (Am. Assoc. Pet. Geol.) Bull. 102 (2), 175–193.
Lai, J., Wang, S., Wang, G., Shi, Y., Zhao, T., Pang, X., Fan, X., Qin, Z., Fan, X., 2019. Pore structure and fractal characteristics of Ordovician Majiagou carbonate reservoirs in Ordos basin, China. AAPG (Am. Assoc. Pet. Geol.) Bull. 103 (11), 2573–2596.
Lai, J., Wang, S., Zhang, C., Wang, G., Song, Q., Chen, X., Yang, K., Yuan, C., 2020. Spectrum of pore types and networks in the deep cambrian to lower ordovician dolostones in tarim basin, China. Mar. Petrol. Geol. 112, 104081.
Li, K., 2010. Analytical derivation of Brooks–Corey type capillary pressure models using fractal geometry and evaluation of rock heterogeneity. J. Petrol. Sci. Eng. 73, 20–26.
Li, K., Horne, R.N., 2003. Fractal characterization of the geysers rock. GRC Trans 27.
Li, K., Horne, R.N., 2006. Fractal modeling of capillary pressure curves for the Geysers rocks. Geothermics 35, 198–207.
Li, Wenhao, Lu, Shuangfang, Xue, Haitao, Zhang, Pengfei, Hu, Ying, 2016. Microscopic pore structure in shale reservoir in the argillaceous dolomite from the Jianghan Basin. Fuel 181, 1041–1049.
Li, Wenhao, Wang, Weiming, Lu, Shuangfang, Xue, Haitao, 2017. Quantitative characterization on shale-hosted oil reservoir: a case study of argillaceous dolomite reservoir in the Jianghan Basin. Fuel 206, 690–700.
Li, Wenhao, Kuang, Yufeng, Lu, Shuangfang, Cheng, Zehu, Xue, Haitao, Shi, Lei, 2019. Porosity enhancement potential through dolomite mineral dissolution in the shale reservoir: a case study of an argillaceous dolomite reservoir in theJianghan Basin. Energy Fuels 33, 4857–4864.
Liu, J., Steel, R.J., Lin, C., Yang, H., Yang, Y., Gong, Y., Peng, L., Chu, C., 2012. Geomorphology control on the development of reservoir depositional systems, Devonian Donghetang formation in the tabei uplift of the tarim basin, China. Mar. Petrol. Geol. 38 (1), 177–194.
Liu, Xiaoping, Jin, Lai, Fan, Xuechun, Shu, Honglin, Wang, Gaocheng, Ma, Xiaoqiang, Liu, Mengcai, Guan, Ming, Luo, Yufeng, 2020. Insights in the pore structure, fluid mobility and oiliness in oil shales of Paleogene Funing Formation in Subei Basin, China. Mar. Petrol. Geol. 114, 104228.
Loucks, R.G., Reed, R.M., Ruppel, S.C., Jarvie, D.M., 2009. Morphology, genesis, and distribution of nanometer-scale pores in siliceous mudstones of the Mississippian Barnett Shale. J. Sediment. Res. 79, 848–861.
Loucks, R.G., Reed, R.M., Ruppel, S.C., Hammes, U., 2012. Spectrum of pore types and networks in mudrocks and a descriptive classification for matrix-related mudrock pores. AAPG (Am. Assoc. Pet. Geol.) Bull. 96, 1071–1098.
Meng, M., Ge, H., Ji, W., Wang, X., 2016. Research on the auto-removal mechanism of shale aqueous phase trapping using low field nuclear magnetic resonance technique. J. Petrol. Sci. Eng. 137, 63–73.
Mitchell, J., Fordham, E.J., 2014. Contributed Review: nuclear magnetic resonance core analysis at 0.3 T. Rev. Sci. Instrum. 85, 1–18, 111502.
Müller-Huber, E., Schön, J., Börner, F., 2016. Pore space characterization in carbonate rocks—approach to combinenuclear magnetic resonance and elastic wave velocity measurements. J. Appl. Geophys. 127, 68–81.
Pape, H., Clauser, C., 2009. Improved interpretation of nuclear magnetic resonance T_1 and T_2 distributions for permeability prediction: simulation of diffusion coupling for a fractal cluster of pores. Pure Appl. Geophys. 166, 949–968.
Rezaee, R., Saeedi, A., Clennell, B., 2012. Tight gas sands permeability estimation from mercury injection capillary pressure and nuclear magnetic resonance data. J. Petrol. Sci. Eng. 88 (89), 92–99.
Sakhaee-Pour, A., Li, W., 2016. Fractal dimensions of shale. J. Nat. Gas Sci. Eng. 30, 578–582.
Schmitt, M., Fernandes, C.P., Wolf, F.G., Neto, J.A.B.C., Rahner, C.P., 2015. Characterization of Brazilian tight gas sandstones relating permeability and angstrom-to micron-scale pore structures. J. Nat. Gas Sci. Eng. 27, 785–807.
Tan, Z., Wang, W., Li, W., et al., 2017. Controlling factors and physical property cutoffs of the tight reservoir in the Liuhe Basin. Adv. Geo-energ. Res. 1 (3), 190–202.
Tavakoli, V., Rahimpour-Bonab, H., Esrafili-Dizaji, B., 2011. Diagenetic controlled reservoir quality of South Pars gas field, an integrated approach. Compt. Rendus Geosci. 343, 55–71.
Wang, H., Liu, Y., Song, Y., Zhao, Y., Zhao, J., Wang, D., 2012. Fractal analysis and its impact factors on pore structure of artificial cores based on the images obtained using magnetic resonance imaging. J. Appl. Geophys. 86, 70–81.
Wang, H., Wu, W., Chen, T., Yu, J., Pan, J., 2019. Pore structure and fractal analysis of shale oil reservoirs: a case study of the Paleogene Shahejie Formation in the Dongying Depression, Bohai Bay, China. J. Petrol. Sci. Eng. 177, 711–723.
Wang, Z., Pan, M., Shi, Y., Liu, L., Xiong, F., Qin, Z., 2018. Fractal analysis of Donghetang sandstones using NMR measurements. Energy Fuels 32, 2973–2982.
Wang, Guiwen, Jin, Lai, Liu, Bingchang, Fan, Zhuoying, Liu, Shichen, Shi, Yujiang, Zhang, Haitao, Chen, Jing, 2020. Fluid property discrimination in dolostone reservoirs using well logs. Acta Geol. Sin. 94 (3), 831–846.
Xiao, D., Lu, Z., Jiang, S., Lu, S., 2016. Comparison and integration of experimental methods to characterize the full-range pore features of tight gas sandstone—a case study in Songliao basin of China. J. Nat. Gas Sci. Eng. 34, 1412–1421.
Yan, Jianping, Zhang, Shaolong, Wang, Jun, et al., 2018. Applying fractal theory to characterize the pore structure of lacustrine shale from the zhanhua depression in bohai bay basin, eastern China. Energy Fuels 32 (7), 7539–7556.
Yan, Jianping, He, Xu, Zhang, Shaolong, et al., 2020. Sensitive parameters of NMR T2 spectrum and their application to pore structure characterization and evaluation in logging profile: a case study from Chang 7 in the Yanchang Formation, Heshui area, Ordos Basin, NW China. Mar. Petrol. Geol. 111 (1), 230–239.
Yang, L., Zhang, X., Zhou, T., Lu, X., Zhang, C., Zhang, K., 2019. The effects of ion diffusion on imbibition oil recovery in salt-rich shale oil reservoirs. J. Geophys. Eng. 16, 525–540.
Zhao, P., Wang, Z., Sun, Z., Cai, J., Wang, L., 2017a. Investigation on the pore structure and multifractal characteristics of tight oil reservoirs using NMR measurements: permian Lucaogou formation in Jimusaer sag, Junggar Basin. Mar. Petrol. Geol. 86, 1067–1081.
Zhang, G.Q., Hirasaki, G.J., House, W.V., 2003. Internal field gradients in porous media. Petrophysics 44 (6), 422–434.
Zhang, K., Lai, J., Bai, G., Pang, X., Ma, X., Qin, Z., Zhang, X., Fan, X., 2020. Comparison of fractal models using NMR and CT analysis in low permeability sandstones. Mar. Petrol. Geol. 112, 104069.
Zhang, J.L., Zhang, P.H., Dong, Z.R., Ding, F., Wang, J.K., Ren, W.W., 2014. Diagenesis of the funing sandstones (Paleogene), gaoji Oilfield, Subei Basin, east of China. Petrol. Sci. Technol. 32 (9), 1095–1103.
Zhang, P., Lu, S., Li, J., Xue, H., Li, W., Zhang, P., 2017. Characterization of shale pore system: a case study of Paleogene Xin'gouzui Formation in the Jianghan basin, China. Mar. Petrol. Geol. 79, 321–334.
Zhang, P., Lu, S., Li, J., Chen, C., Xue, H., Zhang, J., 2018. Petrophysical characterization of oil-bearing shales by low-field nuclear magnetic resonance (NMR). Mar. Petrol. Geol. 89, 775–785.
Zhang, Z., Weller, A., 2014. Fractal dimension of pore-space geometry of an Eocene sandstone formation. Geophysics 79 (6), D377–D387.
Zhao, P., Wang, Z., Sun, Z., Cai, J., Wang, L., 2017b. Investigation on the pore structure and multifractal characteristics of tight oil reservoirs using NMR measurements: permian Lucaogou formation in Jimusaer sag, Junggar Basin. Mar. Petrol. Geol. 86, 1067–1081.
Zhao, Y., Zhu, G., Dong, Y., Danesh, N.N., Chen, Z., Zhang, T., 2017c. Comparison of low-field NMR and microfocus X-ray computed tomography in fractal characterization of pores in artificial cores. Fuel 210, 217–226.
Zhou, L., Kang, Z., 2016. Fractal characterization of pores in shales using NMR: a case study from the lower cambrian niutitang Formation in the middle yangtze platform, southwest China. J. Nat. Gas Sci. Eng. 35, 860–872.